Structures of sodium metal

R. Berliner
Research Reactor, University of Missouri–Columbia, Columbia, Missouri 65211

H. G. Smith
Solid State Division, Oak Ridge National Laboratory, Oak Ridge, Tennessee 37831

J. R. D. Copley
Reactor Radiation Division, National Institute of Standards and Technology, Gaithersburg, Maryland 20899

J. Trivisonno
Department of Physics, John Carroll University, Cleveland, Ohio 44118
(Received 1 August 1991; revised manuscript received 1 June 1992)

The martensitic transformation in sodium metal has been studied using neutron-diffraction and neutron-inelastic-scattering techniques. In two separate experiments the transformation was observed on cooling near 32 K. Measurements of the diffuse scattering, diffraction linewidths, quasielastic scattering, and the temperature dependence of the $\Sigma_4[hh0]$ phonon energies above the transformation show no evidence of transformation precursors. The sodium martensite appears as 24 rhombohedral variants, four about each bcc (110), with reflections from their basal planes at (1.018, 0.92, $\pm$0.06), (0.92, 1.018, $\pm$0.06), and equivalent points. The layer stacking order of the variants is fixed by their relationship to the host bcc material. The crystallography of the low-temperature phase is shown to be a complex mixture of stacking-fault-affected rhombohedral polytypes of a particular "almost-hexagonal" structure. These form a ladder of structures connected, one to another, by stacking faults. As the martensite is warmed and before the complete reversion to a bcc structure, the relative fraction of the different martensite phases changes. Near 55 K, the longest-period polytypes are the most stable.

I. INTRODUCTION

Sodium metal, cooled below about 35 K, abruptly changes its crystal structure from the high-temperature body-centered-cubic to a rhombohedral form. This structural change was recognized as a martensitic transformation in the low-temperature x-ray investigations of Barrett.[1,2] Similar transformations are observed in lithium metal and in many other elements and alloy systems.[3]

Barrett and co-workers, using x-ray diffraction, identified the low-temperature structure of sodium metal as hexagonal-close-packed (hcp) in the absence of cold work. The low-temperature structure of lithium metal was also reported to be hcp. Later neutron-diffraction experiments on polycrystalline lithium[4] were interpreted as evidence that the low-temperature structure was actually the 9*R* rhombohedral stacking polytype.[5] Detailed evidence in support of the 9*R* structure for lithium was obtained from further polycrystalline neutron-diffraction experiments[6] and deviations from the exact 9*R*-stacking diffraction patterns were shown to be the result of high densities of stacking-fault defects.

Recent neutron-diffraction experiments on both lithium and sodium metal have deepened our understanding of the martensitic transformation in the alkali metals. The single-crystal neutron-diffraction experiments by Ernst *et al.*[7] and Smith[8] showed that the low-temperature phase in lithium crystallized in a particular orientation with respect to the parent bcc phase: Peaks corresponding to the diffraction from layers perpendicular to the rhombohedral three-fold axis appear at (1.018, 0.92, $\pm$0.06) and (0.92, 1.018, $\pm$0.06) in the bcc reciprocal space. The new phase exists as 24 variants—four crystallized close to each of the bcc (110) directions. Smith[8] was also able to show that the new phase exhibited 9*R* stacking, but that the displacement of the 9*R* diffraction peaks away from their ideal positions was different from the predictions of the deformation fault model proposed by Berliner and Werner.[6] Subsequent high-resolution polycrystalline neutron-diffraction experiments have confirmed the peak shift pattern observed by Smith in lithium and obtained a similar result for sodium metal.[9]

Displacive structural transformations, such as the ones observed in lithium and in sodium metal are the subject of much current experimental and theoretical interest.[10,11] For many of the systems characterized as "weakly first order," a more or less uniform model has been proposed. This viewpoint is characterized by the experimental results for the NiAl system.[12] As the specimen is cooled, the parent β phase "prepares itself"[11] for the structural transformation. In NiAl, the $\Sigma_4[hh0]$ phonon branch energies are already low and soften further as the specimen is cooled. Elastic diffuse scattering related to the product phase and/or to defects in the parent phase becomes more prominent as the specimen nears the martensitic transformation temperature. These diffuse scattering patterns are the result of fine-scale atomic dis-

placements related to the (Bain) "shear plus shuffle"[13] that converts the bcc lattice to the new hexagonal stacking polytype.

In the case of the alkali metals, this picture is controversial. Blaschko and Krexner[14] studied the diffuse scattering, phonon-dispersion curve and product phase crystallography for the martensitic transformation in sodium metal. They found a few percent softening of the $\Sigma_4[hh0]$ phonon branch in the region from $h \sim 0.3$ to the zone boundary, where reciprocal lattice vectors are defined in the usual manner: $Q = 2\pi(ha^* + kb^* + lc^*)$. This was in comparison to a slight hardening for the remainder of that branch and for the other phonon branches. In addition, they observed a temperature-dependent diffuse scattering above the martensitic transformation temperature, which was attributed to the formation of an intermediate defect structure. Similar effects were observed by Ernst *et al.*[7] in lithium metal. These results are contradicted by other workers,[15–18] who did not observe the phonon anomalies or the pretransition diffuse scattering other than spin-dependent diffuse scattering. Ultrasonic studies of the martensitic phase transformation have also been made in lithium[19] and sodium.[20] No precursor effects in the ultrasonic attenuation or ultrasonic velocity associated with the three independent elastic constants were observed. However, extremely large attenuation changes occur at the martensite start-temperature, M_s.

We report here the results of an extensive study of the martensitic transformation in sodium metal. In Sec. II we describe the crystal preparation and neutron-beam instruments used for this work. In addition, we present the results of a search for transformation precursor phenomena. We measured the diffuse scattering, mosaic widths, quasielastic scattering, and phonon group energies of sodium single crystals as a function of temperature above and below M_s. On two occasions, with two different sodium crystals, we examined the crystallography of the low-temperature phase of sodium metal following the martensitic transformation. These results are also presented in Sec. II. An analysis of the structure of the sodium martensite is presented in Sec. III. It is shown to be a complex mixture of rhombohedral polytypes that form a ladder of structures related by specific stacking faults. Finally, we have examined the thermal stability of the different sodium martensite polytypes as a function of temperature both above and below the martensitic transformation temperature.

II. EXPERIMENT

A. Specimens and neutron spectrometer descriptions

Neutron-diffraction and neutron-scattering investigations were carried out using the BT-9 triple-axis spectrometer at the National Institute of Standards and Technology (NIST) and the 3XE triple-axis spectrometer at the University of Missouri Research Reactor (MURR). At NIST, the BT-9 spectrometer used a pyrolytic graphite monochromator, analyzer, and filter, a wavelength of 2.46 Å, and collimations of 40′-25′-25′-40′. At MURR, only the diffuse scattering above the transformation was investigated. These experiments employed 2.34-Å neutrons. Three sodium single crystals, prepared using standard methods,[21,22] were used for this investigation. In each case, the crystals were oriented with the bcc (001) axis vertical.

B. Search for precursor effects

Measurements of the diffuse scattering, bcc (110) mosaic widths, phonon group energies, and quasielastic scattering were made as the specimens were cooled in stages from 300 K. Figure 1 contains the results of measurements of the bcc (110) rocking curve widths of sodium No. 1 at various temperatures above M_s. The diffraction peak width, in units of h, is observed to increase only slightly as the specimen is cooled.[23] After the transformation, the width of the bcc (110) rocking curve was markedly increased.

The martensitic transformation in lithium metal is signaled by the appearance of reflections from variants of the new phase near the bcc (110) reciprocal lattice points. We monitored the diffracted intensity from sodium No. 1 at (1.018, 0.92, 0) and (0.92, 1.018, 0) with crossed h- and k-scans above the martensitic transformation at $T = 80$ K and at $T = 40$ K. No diffuse scattering structure was observed in these measurements. The counting statistics were sufficient to resolve diffracted intensity changes of 10^{-6} of the bcc (110) peak intensity. The background was observed to increase with decreasing temperature: $I_{40\,K}/I_{80\,K} = 1.07 \pm 0.02$, due to the temperature depen-

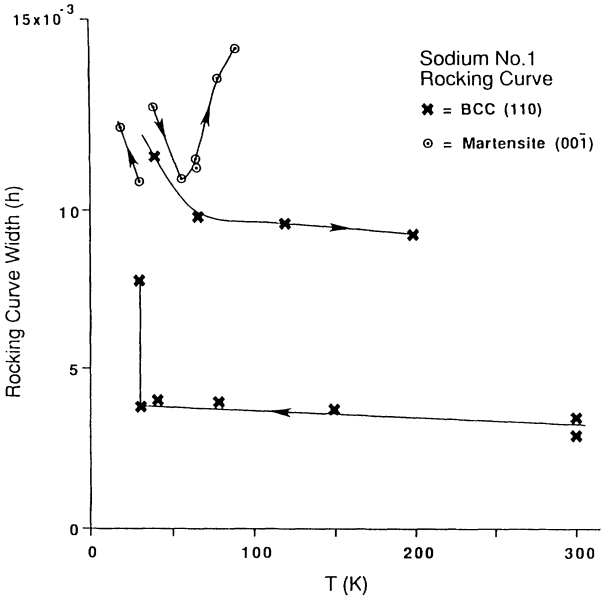

FIG. 1. Rocking curve widths of the sodium bcc (110) and martensite (00$\bar{1}$) as a function of temperature. The diffraction peak widths are presented in units of h: ×, bcc (110); ⊙, (0,0,$\bar{1}$). The martensite phase reflection is indexed in terms of the reduced index L. After the transformation at 32 K, and measurements of the structure of the low-temperature phase, the specimen was cooled to 11 K and then warmed gradually to room temperature. The arrows on the figure indicate warming and cooling branches of the curves.

dence of the spin-incoherent neutron scattering. This intensity ratio is completely consistent with the Debye-Waller factor obtained by Crow *et al.*,[24] which yields $I_{40\text{ K}}/I_{80\text{ K}}=1.06$.

Measurements of the elastic diffuse scattering in various regions of reciprocal space were made at several temperatures above the martensitic transformation using sodium No. 2 and sodium No. 3. A few sharp peaks were observed in these scans, which were confirmed as due to order contamination ($\lambda/2,\lambda/3$).

Measurements of neutron-quasielastic (QE) scattering were made along the bcc reciprocal lattice line (h,1-h,0) for $h=1.5$, 1.45, 1.4, 1.33, 1.2, and 1.1 at various temperatures above the martensitic transformation. In addition, the energy width of the bcc (110) reflection was measured as a function of temperature. No significant change in the energy width of these QE scans were observed.

Measurements of the temperature dependence of the $\Sigma_4[hh0]$ phonon branch are shown in Fig. 2. The motions of atoms corresponding to these phonons are just those that are believed to transform the lattice from a bcc structure to a close-packed-hexagonal (or trigonal) one.[10] Additional measurements of the phonon group energies were made for the zone-boundary phonon, $h=0.5$. Values of the elastic constants and density for sodium as a function of temperature[22] were used to calculate the velocity of sound for comparison to the phonon measurements at low-momentum transfer. The neutron measurements appear to be consistently high at a given h, probably because of resolution effects.[25] Figure 3 shows the energy and width of the neutron groups for the zone-boundary phonon as a function of temperature. The small bars in the figure represent the estimated error in the neutron group energy determination. Similar figures can be drawn for the other points along the curve. Discounting the point at 30 K, after the specimen had

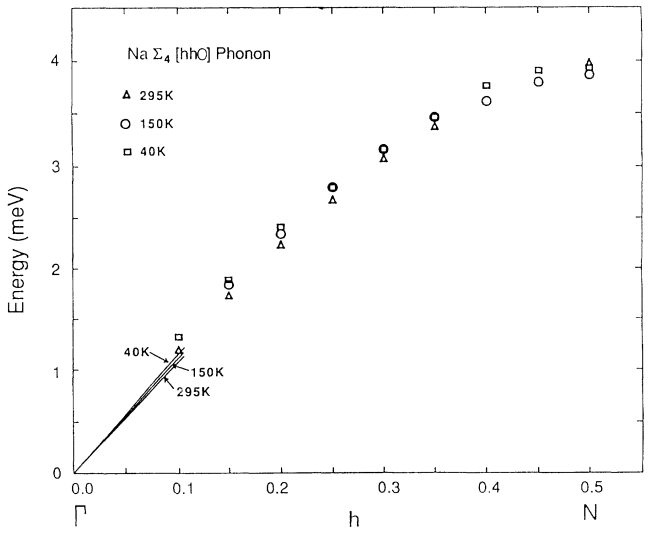

FIG. 2. Dispersion curve for the low-lying transverse acoustic phonon branch ($\Sigma_4[h,h,0]$) at $T=295$, 150, and 40 K before the martensitic transformation. The straight lines drawn from the origin are calculated on the basis of the elastic constants (Ref. 22).

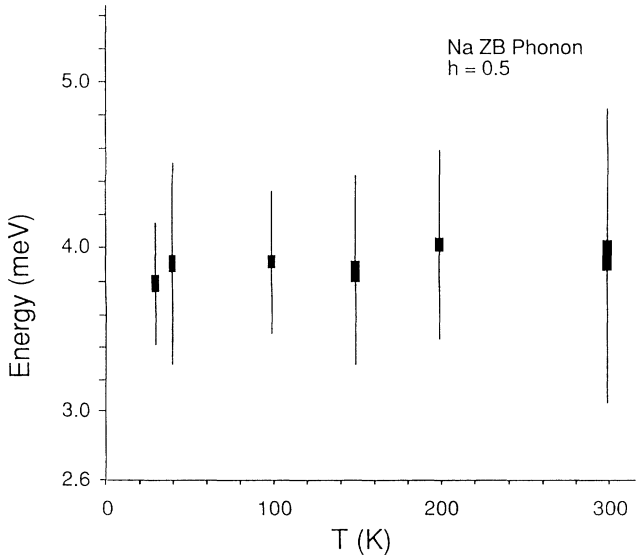

FIG. 3. Energies and neutron group widths (vertical lines) as a function of temperature for the zone-boundary Σ_4 phonon. The small bars represent the estimated error in the energy determination. The measurement at 30 K is difficult to interpret because the crystal has partially transformed to the martensite phase.

partially transformed to the new phase, it is difficult to infer any significant softening of the phonon energies from these data. It is true that even if it is flat, that could be considered anomalous, or at least unusual. However, anharmonic lattice dynamics calculations of Li, Na, K, Rb, and Cs all predict that the N_4' low-lying mode should decrease with decreasing temperature. Many systems behave this way; Pb and Nb are examples. A low-lying zone-boundary mode in TaC, one of the highest melting compounds known, behaves similarly and it is not ready to transform. It is not correct, then, to say that this effect in the alkali metals is a precursor to the martensitic transformation. True first-order transitions do not require it.

C. The transformation and the low-temperature diffraction pattern

In sodium No. 1, the transformation was observed while cooling from 32 to 30 K. The peak intensity of the bcc (110), monitored by successive 2-s counts, was observed to decrease by 40% in the period *between* two measurements (about 4 s).[26] A similarly abrupt transformation was observed with sodium No. 2 at 32 K where the bcc (110) peak intensity decreased 48%. Following the martensitic transformation, reflections from the new phase were observed in the vicinity of the bcc (110) diffraction peak as reported in previous studies of lithium and sodium metal.[7,8,14]

Tilting the bcc crystal axes slightly (±2.5°) revealed two diffraction maxima above and two below the scattering plane. Each maximum is due to diffraction from the hexagonal layer planes of a single variant of the new phase. There are 24 variants in all, four about each bcc

(110). A similar 5° splitting and pattern of intensity was found for the variants observed with sodium No. 2. Measurements of the lattice parameters of the new phase was made with diffraction peaks unaffected by stacking faults. At 32 K, following the transformation, we obtained $a=3.773(8)$ Å and $c=3.080(8)$ Å for the spacing between the layer planes. The bcc lattice parameter at the same temperature was 4.244(4) Å, which gives $V/\text{atom}=38.23$ Å^3 for the cubic and $V/\text{atom}=37.97$ Å^3 for the rhombohedral Na phases.

Figure 4 shows the intensity distribution obtained from a scan along the $(0,1,L)$ of a single variant of the new phase for sodium No. 1. Similar results were obtained for sodium No. 2. The figure is indexed along the c^* axis in terms of the layer spacing instead of the c-axis periodicity so that, for instance, a $9R$ diffraction peak, normally indexed as $(0,1,\bar{4})$ appears as $(0,1,4/9)$. The most prominent features in the diffraction pattern, Fig. 4, show the signature of $9R$ stacking, that is, diffraction peaks appear in the $(0,1,L)$ scan in positions where the equation

$$-h+k+9L=3n, \quad n=0,\pm1,\ldots, \tag{1}$$

is (approximately) satisfied. Similar results are obtained from scans along the $(0,2,L)$ reciprocal lattice line. The presence of significant numbers of stacking twins, as observed, for example, in samarium,[27] would produce peaks not only at points like $(0,1,\bar{4}/9)$ and $(0,1,5/9)$ (as in Fig. 4), but also at points such as $(0,1,4/9)$ and $(0,1,\bar{5}/9)$. Such additional peaks are not observed and we therefore conclude that twinning does not occur in sodium. It is particularly interesting that photographs of the crystal using the bcc $(1\bar{1}0)$ diffracted beam and those from the $9R$ (001) and $(0,1,\bar{4}/9)$ reflections produce reasonably uniform images of the crystal. The variants are not present in distinct (macroscopic) domains, but are spread more or less uniformly throughout the entire specimen.

In addition to the $9R$ component of the diffraction pattern, and in contrast to lithium metal,[28–31] the most striking features of these data of Fig. 4 are the strong shoulders of the $9R$ peaks. They are present near the $(0,1,\bar{4}/9)$, $(0,1,5/9)$, $(0,1,\bar{1}3/9)$, and $(0,1,14/9)$ $9R$ diffraction peaks. Scans perpendicular to $[0,1,L]$ show that the major features of the scattering pattern are centered along this reciprocal lattice line. It seems reasonable to assume that these shoulders are due to yet another martensite phase produced by the transformation. Indeed, additional scattering in the region of the major $9R$ diffraction features was also already noted in the analysis of the polycrystalline diffraction data of Ref. 9. In that work, the additional scattering was tentatively identified as due to a hcp phase fraction with the peak positions shifted and broadened by stacking faults. As we will show below, the single-crystal diffraction pattern requires a more complex interpretation.

The $(0,1,L)$ diffraction peak positions and profiles are complicated by stacking faults as observed in previous experiments on the alkali-metal martensites.[6,8,9] In order to compare the data to a stacking-fault model, we have fit the peaks in the diffraction data in Fig. 4 to Gaussian line shapes. Interpretation of these data is troubled by the well-known difficulty of fitting sets of closely spaced Gaussians to a complex line shape—the results are often not unique. Figure 5(a) contains the comparison of a 3-Gaussian fit to the data in the vicinity of $(0,1,4/9)$, while the 2-Gaussian comparison is shown in Fig. 5(b). For a 3-Gaussian fit, the residual $(R_p=\Sigma|I-I_{\text{calc}}|/\Sigma I)$ is $R_p=0.024$. When these data are fit to two Gaussian lines, $R_p=0.054$. In both cases, the fits represent approximations and the deviations are sufficiently large that a classical goodness-of-fit test is not useful. Attempts to fit these data with sets of two or three Lorentzian line shapes lead to much less satisfactory results.

Study of their geometrical relationships in reciprocal space confirms that overlap of scattering tails from other

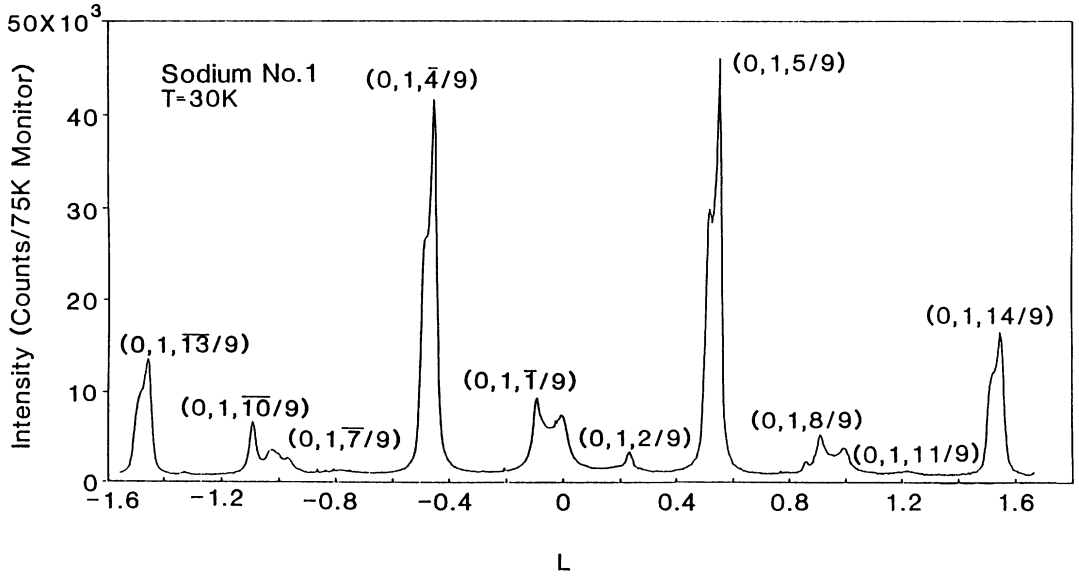

FIG. 4. Diffracted neutron intensity along a martensite variant $(0,1,L)$ axis. The abscissa is in units of the reduced index L. These data, assembled from several consecutive runs, have all been normalized to 75 000 monitor/point which corresponds to 34 s/point.

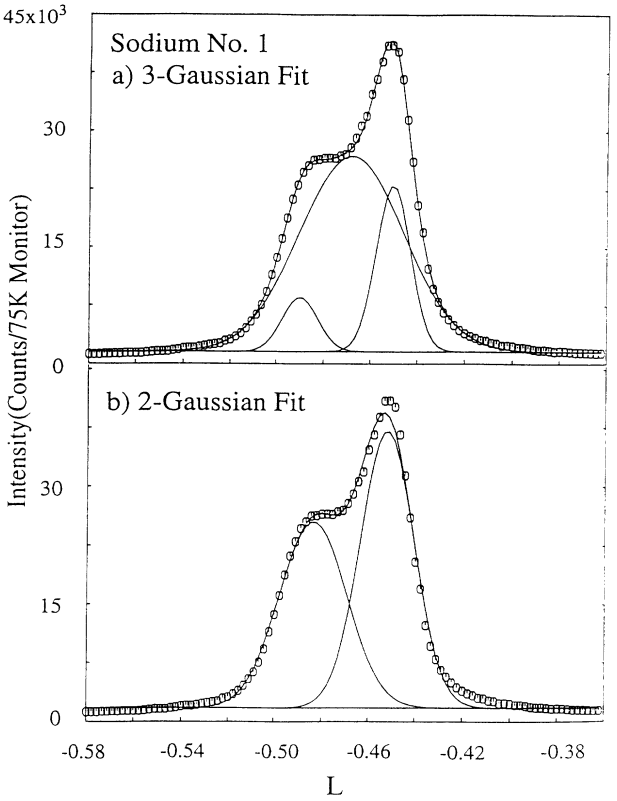

FIG. 5. Examples of least-squares fits to the data of Fig. 4 in the region about $L=-0.47$. Calculated values for the Gaussian components and a flat background are compared to the $(0,1,L)$ diffraction data ⊙: (a) 3-Gaussian fit; (b) 2-Gaussian fit.

variants affects the data in the vicinity of $L=0, \pm 1$. Analysis of the sodium martensite polytype structure must be based, therefore, on the diffraction features near $L=4/9$, 5/9, 13/9, and 14/9. Although the 2-Gaussian fit appears satisfactory for the low-temperature data, the 3-Gaussian fit may be more appropriate to explain the temperature dependence of the data, in addition to explaining other weak peaks.

It is interesting to compare the sodium martensite to the low-temperature structures observed in lithium metal. Schwartz and co-workers[28,29] observed the signatures of mixed $9R$, fcc, and "disordered" polytypes from the diffraction along a $(1,0,L)$ reciprocal lattice line. In their study, the $9R$ diffraction peaks were relatively sharp, while the fcc and other polytypes exhibit high densities of stacking disorder. They attribute a broad diffuse scattering peak near $L=0$ to a hcp phase. A similar mixture of $9R$ and fcc phases was observed by Smith and coworkers,[30,31] although their specimens exhibited lower levels of disorder and a smaller fcc phase fraction, but no evidence of a hcp phase.

III. THE SODIUM MARTENSITE STRUCTURE

In this section we will examine the stacking order and diffraction patterns of long-period polytypes. The results of this investigation in combination with the sodium martensite $(0,1,L)$ and $(0,2,L)$ diffraction data will be used to suggest candidate polytypes for the sodium structure. We will discuss the nature of stacking-fault defects in these crystal structures and explore the effect of defects on their diffraction patterns. Finally, we will use these developments to show how stacking-fault defects in combination with different rhombohedral polytype base sequences can be used to approximate the measured sodium $(0,k,L)$ diffraction patterns.

A. Long period rhombohedral polytypes

The positional asymmetry of the $9R$ diffraction peak shoulders in the $(0,1,L)$ and $(0,2,L)$ diffraction data requires the new martensite phase to be rhombohedral—a general hexagonal stacking would have a diffraction pattern symmetric about $L=0$. The c-axis period (in terms of the layer spacing) must then be divisible by 3 and the possible (rhombohedral) c-axis periodicities are $3,9,12,\ldots,3n$ layers.[32]

It is fortunate that the new phase must have a rhombohedral stacking sequence because there is an enormous variety of combinatorially possible hexagonal stacking sequences even for relatively short c-axis periodicities.[6] In order to identify the structures responsible for the additional diffraction features in the sodium data, it is useful to discuss the polytype sequences in terms of the Zhdanov notation.[33]

Consider a general hexagonal-layer stacking pattern such as the 10-layer sequence: $\cdots C/ABCBACACBC/A\cdots$. If the transitions, moving from left to right, from an A to a B to a C layer, are considered to be "positive" $(+)$, and transitions in the opposite direction "negative" $(-)$, then the sequence can be labeled as: $\cdots +/++---+--++/+\cdots$. When the plus and minus symbols are gathered together, the sequence is written as (23122), where the numbers in the symbol are the numbers of successive alternating positive and negative transitions in the stacking sequence. Once a sequence is expressed in this fashion, it is found that a rhombohedral sequence must consist of three sets of $N/3$ layers, and that for each set,

$$n_+ - n_- = \pm 3r \pm 1 \ , \tag{2}$$

where n_+ and n_- are the numbers of "+" and "−" layers in a set of $N/3$ layers, N is the c-axis periodicity, and r, an integer.[33] Equation (2) expresses the condition that the layer type of corresponding layers in each set of $N/3$ is cyclically permuted from A to B to C. It can be simply solved, using $n_+ + n_- = N/3$, to yield the number of n_+ and n_- layers in a particular rhombohedral $N/3$ subsequence. For each value of n_+, and the corresponding n_-, there are a number of different possible stacking sequences. For instance, for $N/3=9$ $(27R)$, there is only one (unique) stacking sequence that corresponds to $n_+=8$; $(n_+ n_-)_3=(81)_3$. On the other hand, there are four sequences that arise from $n_+=7$: $(72)_3$, $(6111)_3$, $(5121)_3$, and $(4131)_3$.[34] The complete set of unique rhombohedral stacking sequences for $N\leq 27$ is listed in Table I.

If the period of the rhombohedral sequence is N, the

positions of diffraction spots along the $(0,1,L)$ will obey a rule similar to that of Eq. (1) and appear at positions given by

$$L=(3n-1)/N, \quad n=\pm 0,1,2,\ldots . \tag{3}$$

An approximate solution to Eq. (3), using the position for the diffraction shoulders given by the 3-Gaussian decomposition, is obtained with $N=51$. The diffraction feature in the decomposition [Fig. 5(a)] at $L=-0.490$ would then be attributed to a $(0,1,25/51)$ diffraction peak of the $N=51$ rhombohedral polytype. If the diffraction peak positions of this new low-period polytype phase have been shifted by stacking faults, the observed peak position is probably the result of diffraction from a stacking-fault-affected polytype of period shorter than 51. If the position of the shoulder is taken from the 2-Gaussian decomposition [Fig. 5(b)], an approximate solution is obtained with $N=27$ and this feature is attributed to the $(0,1,\bar{1}3/27)$ peak of a $27R$ polytype. In either case, it is useful to investigate the diffraction shoulders under the assumption that $N=27$. The intensity at $L=-0.490$ would then arise from the stacking-fault-shifted $(0,1,\bar{1}3/27)$ peak of this $N=27$ rhombohedral polytype.

The calculated $(0,1,L)$ diffraction patterns for the $27R$ stacking sequences listed in Table I are shown in Fig. 6. The stacking sequences vary from the $(21111111)_3$, which consists of one K (cubic) layer every 9 layers to the $(81)_3$ stacking in which nearly all the layers have a cubic environment. The other diffraction patterns are intermediate in some sense, but they do not go "smoothly" from one

TABLE I. Rhombohedral stacking polytypes $N\leq 27$. A summary of the rhombohedral stacking sequences for $N\leq 27$ is shown below. The quantity N is the length of the unit cell along the c axis in terms of the layer spacing. Also listed for the sequences are the Zhadanov symbol, Jagodzinsky (H-K) notation, and traditional A-B-C layer designation. The vertical lines separating letters in the A-B-C representation show the $N/3$ rhombohedral fragment of the sequence.

N	Zhadanov symbol	Jagodzinsky	Sequence
3	$(1)_3$	K	$C\|A\|B$
9	$(21)_3$	HKH	$B\|ABC\|B$
12	$(31)_3$	$KKKH$	$C\|ABCA\|C$
15	$(32)_3$	$HKKHK$	$B\|ABCAC\|B$
	$(2111)_3$	$HKHHH$	$B\|ABCBC\|B$
18	$(51)_3$	$HKKKKH$	$B\|ABCABC\|B$
	$(42)_3$	$HKKKHK$	$B\|ABCABA\|C$
	$(3111)_3$	$HKKHHH$	$B\|ABCACA\|C$
21	$(61)_3$	$HKKKKKH$	$B\|ABCABCA\|C$
	$(43)_3$	$HKKKHKK$	$B\|ABCABAC\|B$
	$(2221)_3$	$HKHKHKH$	$B\|ABCBABC\|B$
	$(3211)_3$	$HKKHKHH$	$B\|ABCACBC\|B$
	$(211111)_3$	$HKHHHHH$	$B\|ABCBCBC\|B$
24	$(62)_3$	$HKKKKKHK$	$B\|ABCABCAC\|B$
	$(5111)_3$	$HKKKHHHH$	$B\|ABCABCBC\|B$
	$(4121)_3$	$HKKHHHKH$	$B\|ABCABABC\|B$
	$(53)_3$	$HKKKKHKK$	$B\|ABCABCBA\|C$
	$(3221)_3$	$HKKHKHKH$	$B\|ABCACBCA\|C$
	$(4211)_3$	$HKKKHKHH$	$B\|ABCABACA\|C$
	$(311111)_3$	$HKKHHHHH$	$B\|ABCACACA\|C$
	$(212111)_3$	$HKHHKHHH$	$B\|ABCBCACA\|C$
27	$(81)_3$	$HKKKKKKKH$	$B\|ABCABCABC\|B$
	$(72)_3$	$HKKKKKKHK$	$B\|ABCABCABA\|C$
	$(6111)_3$	$HKKKKKHHH$	$B\|ABCABCACA\|C$
	$(54)_3$	$HKKKKHKKK$	$B\|ABCABCBAC\|B$
	$(5121)_3$	$HKKKKHHKH$	$B\|ABCABCBCA\|C$
	$(4212)_3$	$HKKKHKHHK$	$B\|ABCABACAC\|B$
	$(4311)_3$	$HKKKHKKHH$	$B\|ABCABACBC\|B$
	$(4131)_3$	$HKKKHHKKH$	$B\|ABCABABCA\|C$
	$(3321)_3$	$HKKHKKHKH$	$B\|ABCACBABC\|B$
	$(3222)_3$	$HKKHKHKHK$	$B\|ABCACBCAC\|B$
	$(321111)_3$	$HKKHKHHHH$	$B\|ABCACBCBC\|B$
	$(311211)_3$	$HKKHHHKHH$	$B\|ABCACACBC\|B$
	$(222111)_3$	$HKHKHKHHH$	$B\|ABCBABCBC\|B$
	$(212211)_3$	$HKHHKHKHH$	$B\|ABCBCACBC\|B$
	$(21111111)_3$	$HKHHHHHHH$	$B\|ABCBCBCBC\|B$

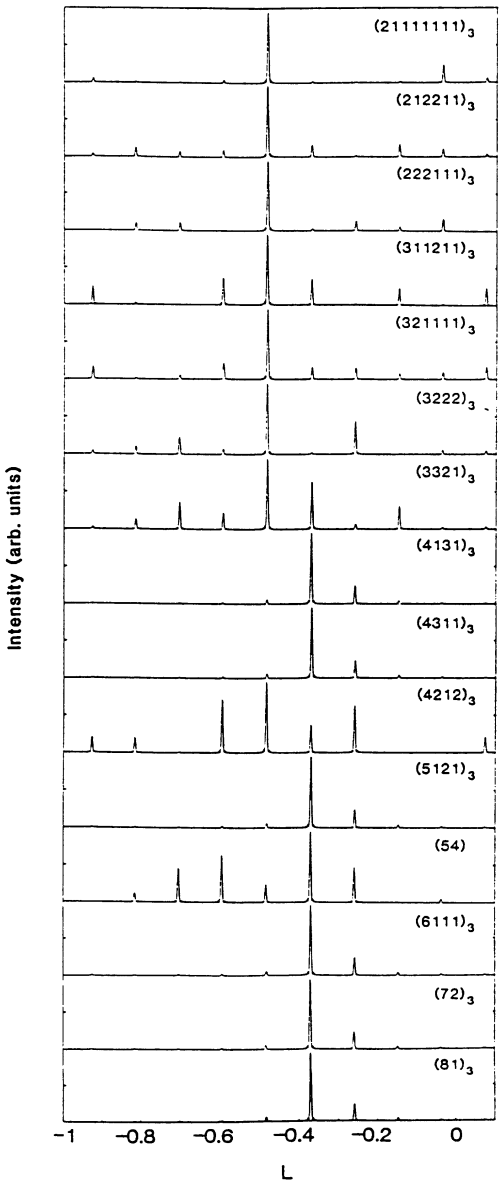

FIG. 6. Calculated diffraction patterns for all the possible $27R$ stacking polytypes in terms of the reduced index L over the region $-1\leq L\leq 0$.

to the next as the number of hexagonal layers is varied. Of the 15 27R diffraction patterns, only that due to the $(21111111)_3$ is sufficiently similar to the sodium $(0,1,L)$ diffraction data to merit further consideration. The calculated patterns for the $(21111111)_3$ stacking shows a strong peak at $L=-\frac{13}{27}$, a moderately strong line at $L=-\frac{1}{27}$ and a weak feature at $L=-\frac{25}{27}$. All of the other diffraction patterns show strong or moderately strong diffraction peaks in regions where no similar features are observed in the sodium data.

The 27R-$(21111111)_3$ stacking is one of a family of "almost-hexagonal" rhombohedral polytypes. The diffraction patterns for this family of polytypes are interesting and are shown in Fig. 7. They typify a staircase structure whose diffraction patterns approach an hcp or fcc pattern as the number of hexagonal layers increases or decreases. The sodium lattice appears to assume a mixture of these structures as it is warmed following the martensitic transformation.

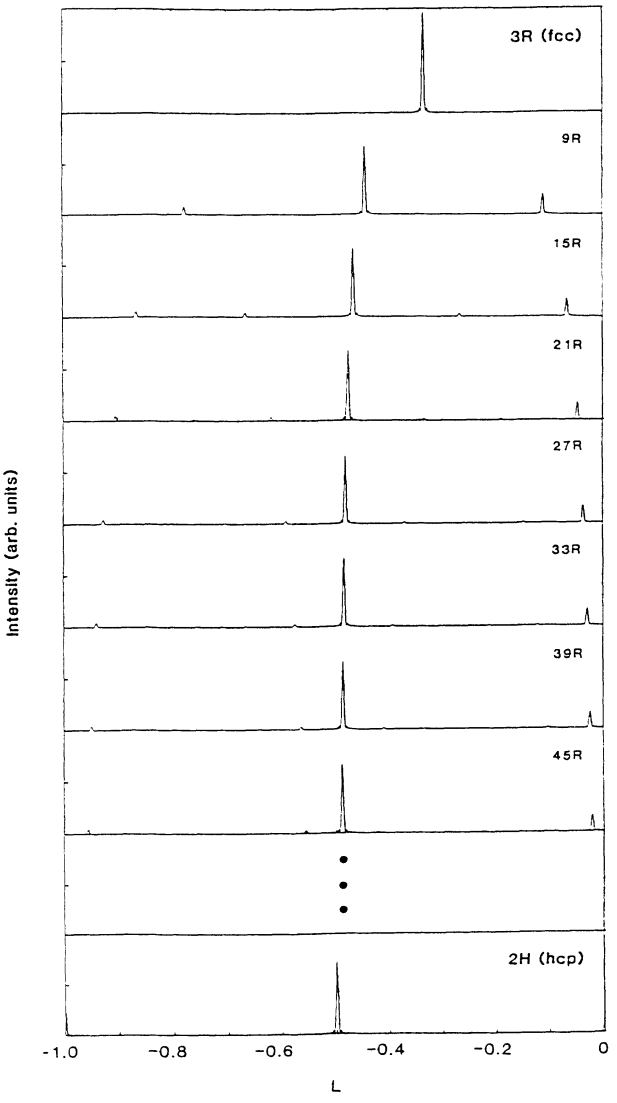

FIG. 7. Calculated diffraction patterns in terms of the reduced index L over the range $-1\leq L\leq 0$ for the "almost-hexagonal" polytypes, nR, for $n\leq 45$. The 2H (hcp) diffraction pattern is shown for comparison.

B. Stacking faults in "almost-hexagonal" polytypes

Under the assumption that the diffraction peaks of the long-period polytypes are affected by stacking faults, the absence of symmetry about $L=0$ in the diffraction pattern (Fig. 4) demands that the defects responsible be "nontwinning."[35] In analogy to the treatment of stacking faults in Ref. 9, we can work out a table of "jump faults" for the long-period almost-hexagonal polytypes. There is only one kind of jump fault in the 3R (fcc) lattice while there are, respectively, 9, 26, 51, and 80 different kinds of nontwinning stacking faults in the 9R, 15R, 21R, and 27R lattices. In a crystal of a particular polytype, stacking faults are distinguished by their insertion sequences, i.e., the sequence of layers that interrupts the perfect crystal stacking. For topological reasons, certain stacking faults can occur only at particular sites within the unit cell. In the 15R-$(2111)_3$ polytype for example, the fault that results in an inserted -HH- sequence can occur at each layer of the cell, while the one that produces an inserted -KK- sequence can occur at only six sites/unit cell. It is interesting that the most probable defects act as "creation" and "annihilation" operators on the stacking sequence. For instance, in the 15R polytype, the most probable defects produce -HH- and -KHH- insertions that create the $N/3$ fragment of the next higher (21R) and next lower (9R) stacking sequences. The next most probable defects create the -K- and -$HHHH$- sequences that produce the $N/3$ fragment of the 3R and 27R stackings. Analogous results are obtained for the other long-period almost-hexagonal polytypes.

It is not obvious that these stacking faults are indeed produced by the "jump" mechanism described above. Gooding and Krumhansl[10] have explored a mechanism for the martensitic transformation in lithium metal that

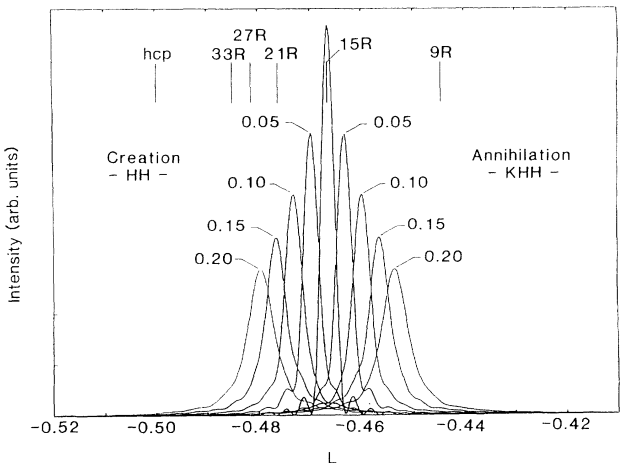

FIG. 8. Calculated diffraction pattern for the region about $L=-0.47$ for the 15R "almost-hexagonal" lattice and different concentrations of "creation" and "annihilation" stacking faults. The concentrations corresponding to each case and the diffraction peak positions for the perfect crystal 9R, 15R, 21R, and 27R lattices are marked on the figure.

results in short twinned regions in the normal $9R$ stacking sequence. When the length of the twinned region is reduced to one layer, Gooding's twin is recognized as the defect responsible for the diffraction peak shifts observed in the alkali-metal martensites,[9] these single-layer double-twin faults are the same as the -*HH*- inserting jump faults in the $15R$-$(2111)_3$ lattice. It does not appear possible to introduce the "annihilation" sequences such as -KH_2- or -*K*- by a similar double-twin mechanism. Instead, the only recourse seems to be the introduction of this type of defect by shear deformation induced dislocations.

Using the Monte Carlo techniques described in Refs. 6 and 9, we investigated the effect of the stacking faults on the $(0,1,L)$ diffraction patterns of the almost-hexagonal $9R$, $15R$, $21R$, and $27R$ polytypes. Figure 8 illustrates the most important result of these calculations—the effect of stacking faults which insert -H_2- sequences and -KH_2- sequences on the $(0,1,\overline{7/15})$ diffraction peak of a $15R$-$(2111)_3$ polytype. The sequence-lengthening stacking faults, i.e., those that result in the -H_2-, -H_4- or -H_6- insertions, cause the $L=-\frac{7}{15}$ diffraction peak to shift toward $L=-\frac{1}{2}$. The sequence-shortening faults, i.e., those that produce -KH_2- and -*K*- insertions, cause the prominent $L=-\frac{7}{15}$ diffraction peak to shift toward $L=-\frac{1}{3}$. The less intense diffraction peak, at $L=-\frac{1}{15}$, is similarly shifted toward $L=0$ by the sequence-lengthening insertions and toward $L=-\frac{1}{3}$ by the sequence-shortening ones. The $L=-\frac{13}{15}$ diffraction peak, which is already the weakest, is strongly broadened by either defect type.

C. The sodium structure model

We assume, in accordance with the diffraction data and neutron photographs, that the martensite phase consists of a large number of microscopic rhombohedral-structure domains. The *c* axis and stacking order of each of these domains is fixed by its relationship to the host bcc lattice. Two alternative models for the sodium martensite can be constructed. One, corresponding to the 3-Gaussian decomposition of the $(0,1,L)$ diffraction data [Fig. 5(a)], invokes three ensembles of domains for each variant. The diffraction pattern of each ensemble corresponds to one of the three features from the decomposition of the diffraction data and has a characteristic distribution of stacking faults and polytype lengths. We identify these three ensembles with the stacking-fault distorted $9R$, $15R$, and $45R$ almost-hexagonal stackings. The alternative 2-Gaussian decomposition of the $(0,1,L)$ diffraction data leads to a model consisting of stacking-fault-shifted and -broadened $9R$ and $27R$ components. In both models, the positions of these diffraction features change with temperature. The shifts are sufficiently large to cause us to identify these features, at higher temperatures, with other stacking sequences and to denote them as the short-, medium-, and long-period components.

It is tempting to attribute the scattering near $(0,1,0)$ in Fig. 4 to a hcp phase fraction but this interpretation must be rejected. First, there is no corresponding feature in the diffraction data at $L=\pm 0.5$ which would be the signature of the hcp lattice. Second, it is not possible to shift the position of the hcp diffraction peaks away from $L=0$, ± 0.5 by any set of randomly introduced stacking faults. Monte Carlo calculations of stacking-fault-distorted hcp lattices performed by one of us and analytical examinations of the effect of stacking faults in hcp crystals confirm that only peak broadening will result.[35,36–38]

The effect of stacking faults on the $9R$ polytype has been discussed in Refs. 6 and 9 and we have demonstrated similar results for the $15R$ and longer polytypes. Therefore, a suitable choice of the underlying "almost-hexagonal" rhombohedral polytype along with the appropriate density of random creation faults is used in our model to place the diffraction peaks at the observed positions along the $(0,1,L)$ reciprocal lattice line. Additional creation and annihilation faults, added in appropriate proportions, serve to broaden the peaks in the diffraction pattern. A further source of diffraction peak broadening is the transformation-induced mosaic and strain that is seen in the width of the trigonal $(0,0,\overline{1})$ and bcc (110) diffraction peaks following the martensitic transformation. In order to account for these effects, the calculated diffraction patterns have been convoluted with a Gaussian of width $\delta L=0.0062$, which is commensurate with the observed width of the stacking-fault-unaffected diffraction peaks. Finally, the heights of the calculated intensity distributions have been adjusted to the data, represented by the decompositions of Fig. 5, and the diffracted intensities for the component ensembles summed.

Using the Monte Carlo modeling techniques,[6,9] and the prescription outlined above, models of the sodium martensite structure were constructed starting from the 3-Gaussian and 2-Gaussian decompositions of the diffraction data. Figure 9 compares the sodium $(0,1,L)$ diffraction data with the diffracted intensities calculated using the three-component and two-component models. Suitable agreement is guaranteed near $L=-\frac{4}{9}$ and $L=\frac{5}{9}$ because the individual model intensity distributions are scaled to the decompositions of the data. The concordance between the data and both models is somewhat less satisfactory in the region near $L=0$ and $L=\pm 1$.

It is important that the $(0,1,L)$ diffraction patterns observed near $L=\pm 1$ and $L=0$ are significantly different. This argues that these regions of the diffraction pattern are contaminated by the overlap of scattering from the different martensite variants and diffraction from the untransformed bcc material. These effects can be understood with reference to the (rather crowded) reciproal space of sodium metal below the martensitic transformation. Omission of the Debye-Waller effect in the diffracted intensity calculation also contributes to the discrepancy.

The 3-Gaussian model indicates that the major portions of the martensite phase are highly disordered $15R$ (84%) and $45R$ (3%) almost-hexagonal polytypes. The remainder (13%) is a lightly disordered $9R$ polytype with $P_c=0.072$ and $P_a=0.018$ for the probability per layer for creation and annihilation faults. The 2-Gaussian model shows 28% of the martensite as the $9R$ polytype with

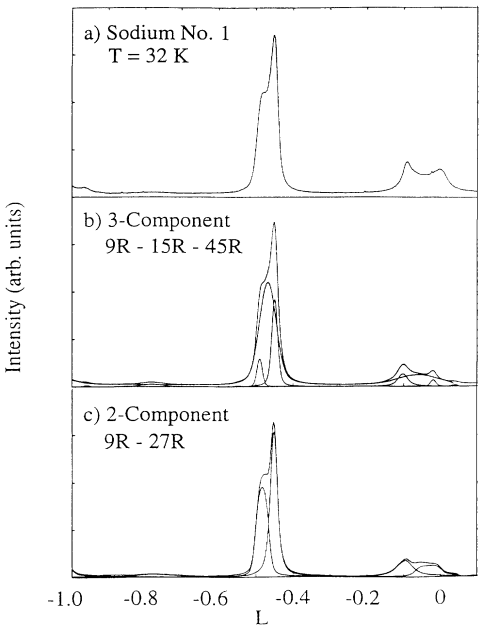

FIG. 9. Calculated diffracted intensities from the different sodium structural models are compared to the $(0,1,L)$ sodium martensite diffraction data: (a) the diffraction data for sodium No. 1 at 32 K; (b) the three-component model calculated intensity; (c) the two-component model calculated intensity. The diffraction patterns for each of the model components and their sums are displayed.

72% present as a highly disordered $27R$ polytype. In spite of the qualitative success of the models, we recognize that they still represent incomplete descriptions. For example, it is likely that our use of only two different kinds of stacking faults represents a gross simplification. In the absence of additional detailed microscopic information, such as that obtained from electron microscopy, it is not possible to discriminate further among the possible "nontwinning" defect types or bases sequences. The essential features of the structural models: the almost-hexagonal polytypes and the presence of large numbers of creation and annihilation stacking faults are common to both representations of the low-temperature sodium structure.

D. The reverse transformation: Annealing the martensite

The reversion of the martensite phases to bcc was monitored as a function of temperature for sodium No. 1 and sodium No. 2. In both cases, the relative fraction of the different polytypes was observed to change. Different time-temperature schedules were followed in the two experiments. Sodium No. 1, which had been held for ~60 h at 32 K, was first cooled to 9.4 K, and then warmed, over the course of 30 min, to 40 K. Subsequent measurements were made at 55, 65, 80, and 90 K. Sodium No. 2 was warmed from 32 K in stages to 55 K, cooled again to 32 K, pulse annealed for ~60 min at 55 K and then cooled to 11 K. The complicated time-temperature schedule for sodium No. 2 was an unsuccessful attempt to create a "single-phase" martensite specimen.

Some results of diffracted intensity measurements along the martensite $(0,1,L)$ as a function of temperature are shown in Fig. 10 for sodium No. 1. The inset in the figure shows a schematic time-temperature profile for this experiment. The peak positions from the 3-Gaussian decomposition of these data, as described for Fig. 5(a), are plotted in Fig. 11. The positions of the prominent diffraction peaks for the perfect crystal almost-hexagonal polytypes are marked at the side of the figure. As the specimen was warmed above 40K, the long-period component shifted somewhat closer to the hcp diffraction peak position, while the broad central diffraction feature locked in at the position corresponding to a $21R$ polytype diffraction peak. Nearly identical results were obtained for the diffraction peak positions of sodium No. 2 as it was warmed from 32 to 55 K.

The integrated intensities of the diffraction peaks obtained from the 3-Gaussian decomposition of the data of Fig. 10 are shown in Fig. 12(a) for sodium No. 1 and the first part of the time-temperature schedule of the integrated intensities for sodium No. 2 is shown in Fig. 12(b). The relative fractions for the martensite components present in each specimen at low temperature are different, probably due to the well-known sample dependence of the martensitic transformation, but the behavior of the two specimens on warming is quite consistent. As the crystal is warmed above 40 K, the short-period component fraction is observed to steadily decrease while the medium-period fraction is seen to have a sharp annealing stage between 50 and 60 K. In both experiments, the long-period polytype phase fraction is observed to grow in the region 40–60 K. As the martensite is warmed still further, the $9R$ phase fraction disappears, leaving the broadened $21R$ polytype and a long-period component. Above 90 K, the crystal was substantially converted back to the bcc structure with the original orientation.

If the data of Fig. 10 are described instead by a 2-Gaussian decomposition, the position of the short-period component shifts from approximately $9R$ ($L=0.4540$) at

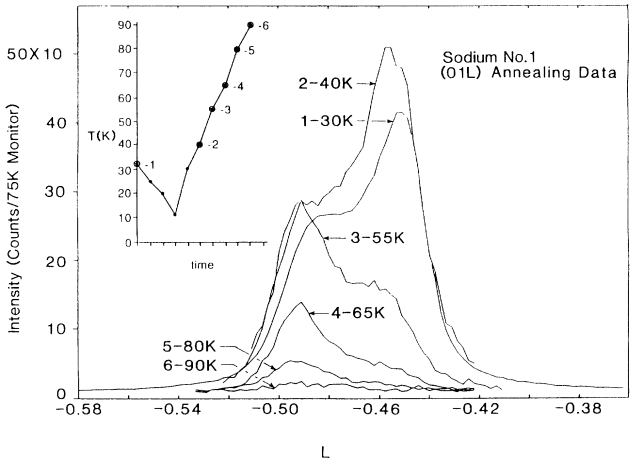

FIG. 10. Neutron-diffraction intensity along the martensite $(0,1,L)$ at various temperatures for sodium No. 1. The inset in the figure is a schematic diagram of the time-temperature profile.

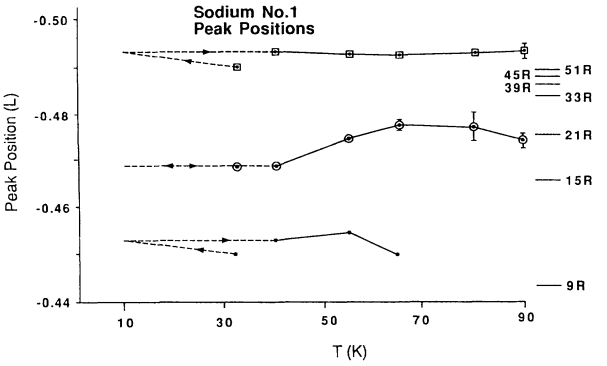

FIG. 11. Diffraction peak positions as a function of temperature on warming for sodium No. 1 obtained from the 3-Gaussian decomposition of the data of Fig. 10. ●, Short-period component; ⊙, medium-period component; ⊡, long-period component. The positions of the perfect crystal diffraction peaks for several rhombohedral polytypes are shown in the figure. The dashed lines show the likely path of the component peak positions as the specimen was cooled to 9 K and warmed to 40 K.

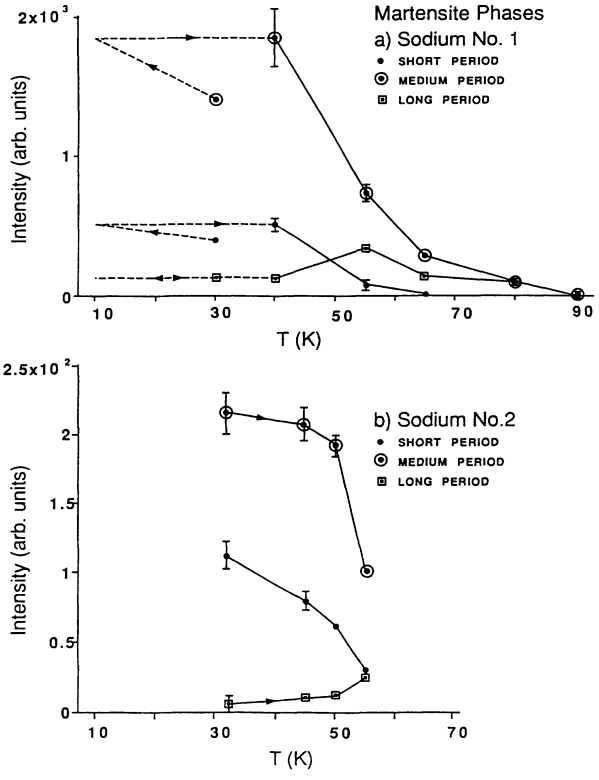

FIG. 12. Integrated intensities for the components of the sodium martensite. ●, Short-period component, ⊙, medium-period component; ⊡, long-period component. (a) Sodium No. 1. Following the transformation at 32 K, the specimen was cooled to 9 K and then warmed to 35 K. The dashed lines show the likely path of the integrated intensities for $T < 35$ K. (b) Sodium No. 2. After the transformation at 32 K, the specimen was warmed to 55 K in stages.

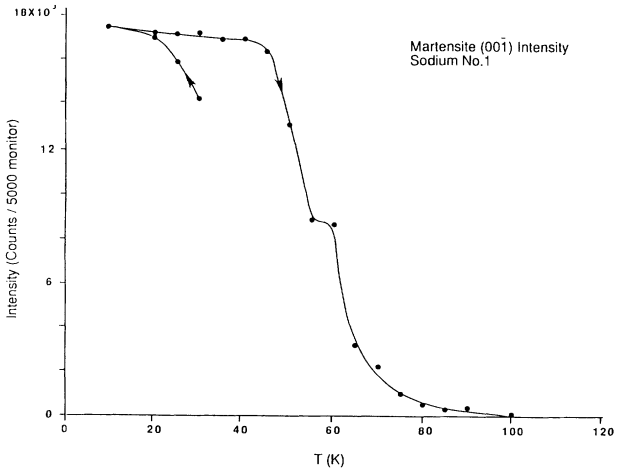

FIG. 13. Diffracted intensity at the martensite $(0,0,\bar{1})$ as a function of temperature. Arrows on the figure show the branches of the curve that correspond to cooling and warming.

32 K to approximately $21R$ ($L = 0.4750$) as the specimen is warmed to 90 K. At the same time, the long-period component is displaced from near $39R$ ($L = 0.483$) to above $51R$ ($L = 0.4940$). The integrated intensities in this interpretation both decrease as the specimen temperature is increased, with the short-period component showing the faster reversion to bcc between 40 and 65 K.

A view of the reversion of all the martensite phases to bcc is given by Fig. 13, which shows the peak intensity of the martensite $(0,0,1)$ as a function of temperature. Arrows on the figure indicate the branches of the curve that correspond to cooling and warming of the specimen. The data exhibit a shoulder at 55 K where the mosaic width of the martensite $(0,0,\bar{1})$ (Fig. 1) passes through a minimum.

Final warming to room temperature for each specimen was done in careful stages in an attempt to prevent loss of the crystal. The warming for sodium No. 1 was performed over the course of several hours. The fact that the bcc (110) mosaic widths remain large as the specimen is warmed is evidence that the transformation-induced stresses have not been relieved. Nevertheless, the specimen remained a bcc single crystal with the original orientation until between 250 and 300 K, where it "broke" into several distinct grains. In the case of sodium No. 2, warming proceeded in 20-K steps, starting at 11 K, and pausing 45 min at each temperature. This specimen transformed into several grains about 30 min after the temperature was raised to 270 K. Similar effects were observed in the ultrasonic study in sodium,[20] but not in lithium,[19] which generally exhibited the shape memory effect and transformed back to a single crystal with the same orientation. Stedman also reported a similar loss of his sodium crystal, on warming, following the martensitic transformation.[18]

IV. SUMMARY AND CONCLUSIONS

As with the transformation in lithium metal, reflections from the martensite phase in sodium appear at

(1.018, 0.92, ±0.06), (0.92, 1.018, ±0.06), and equivalent points in the bcc reciprocal lattice. These reflections correspond to diffraction from the hexagonal-layer planes of the rhombohedral martensite structure. There are four variants associated with each bcc (110), 24 variants in all, and they are not equally populated. The transformation was observed in both specimens at about 32 K.

The crystalline morphology of the sodium martensite is remarkable. Studies of the martensitic transformation in polycrystalline sodium[9] indicate that only 43% of the specimen transforms, the remainder retaining the bcc structure. The variants coexist with each other and with the remaining bcc material on a microscopic scale without a distinct grain structure. Microscopic regions of the crystal, oriented in the same manner with respect to the bcc lattice, belong to the same variant and adopt the same stacking order. Each variant adopts a particular stacking order and contains no twins. It appears that the two variants at (1.018, 0.92, ±0.06) have the same stacking sequence, which is opposite to the stacking order of the pair at (0.92, 1.018, ±0.06).

We were unable to identify any precursors of the transformation at temperatures above M_s. Scans at several temperatures along high-symmetry directions showed no significant evidence of unexplained additional scattering. No additional scattering near the martensite condensation point, (1.018, 0.92, 0), was observed at 150, 80, and 40 K before the transformation. A general rise in the diffuse scattering with a reduction in temperature is attributed in the Debye-Waller increase of the spin-incoherent *elastic* scattering. No anomalies were observed in studies of the quasielastic scattering as a function of temperature above the transformation.

Incomplete phonon softening is often cited as the mechanism for spontaneous structural phase transformations.[39–41] Our measurements do not support this model in the case of sodium metal. We studied the dispersion relation of the $\Sigma_4[h,h,0]$ transverse acoustic phonon branch as a function of temperature to confirm reports of softening, (within experimental error), at the zone boundary or elsewhere in the zone, which have been reported by some workers[14] and are invoked in theoretical treatments.[10] The unusual behavior of the temperature dependence of this branch compared to the other branches is predicted for Na and all the other alkali metals by anharmonic calculations, and this behavior has been observed in other materials that do not transform, e.g., Pb, Nb, and TaC.

Following the martensitic transformation, we find the sodium metal is composed of a complex mixture of rhombohedral polytypes. We interpret the low-temperature diffraction data in terms of stacking-fault-affected $9R$ (short-period), $15R$ (medium-period), and $45R$ (long-period) almost-hexagonal polytypes or in terms of a two-component $9R$ and $27R$ model. The unit cell for an almost-hexagonal polytype consists of three sequences of layers, each of which contains a single layer with a cubic environment followed by an even number of layers with hexagonal environments.

The effects of stacking faults on the features corresponding to the polytype component diffraction peaks can be seen in the peak positions and peak widths obtained from the decompositions of the data. They are displaced from their expected positions and broadened. The absence of stacking twins in these data demands that the layer defects responsible be non-twinning. An exhaustive study of stacking faults that satisfy this requirement clarified the nature of nontwinning defects in long-period polytypes and showed that the combinatorially most likely are the "creation" and "annihilation" faults. These stacking faults connect the almost-hexagonal rhombohedral polytypes in a ladder of structures and provide a simple mechanism for converting one polytype to another.

A model for the sodium martensite, based on stacking-fault-affected $9R$, $15R$, and $45R$ stacking sequences or, equivalently, on $9R$ and $27R$ sequences, provides a good approximation to the diffraction data. These models assume that the martensite is composed of ensembles of crystallites, each ensemble with its own basic stacking sequence and distribution of stacking-fault defects. Diffracted intensity calculations for the two models yield slightly different results in the vicinity of $L=0$, ±1, ±2,.... Although either model appears to fit the low-temperature data, the 3-Gaussian model appears to fit the temperature dependence of the scattering intensity somewhat better. It is possible that high-resolution diffraction measurements or study of single variant specimens would avoid overlap effects and distinguish between these two representations.

We find that the relative fraction of the different sodium martensite phases is sample dependent and changes as the specimen is warmed or cooled following the transformation. Cooling the crystals well below M_s increases the relative amount of the $9R$ (short-period) phase fraction at the expense of the bcc phase. As the specimen is warmed, there are changes in the position and intensities of the diffraction features, indicating changes in their underlying stacking sequences or in the relative number of creation and annihilation faults in the members of the different crystallite ensembles. These effects argue that the longer-period polytypes are more stable in the range 45–60 K. This is interesting in view of the fact that the behavior in lithium metal is just the opposite--the short-period (fcc) polytype appears to be more stable as the martensite is warmed.[17,28–31]

Recent pressure experiments[42] on polycrystalline samples of sodium showed that the transition could be suppressed by application of modest hydrostatic pressures (a few kilobars) whereas, in lithium, the application of pressure[17] actually increased M_s. However, the effects on stacking-fault behavior could not be ascertained for either element; single-crystal studies under pressure will be required.

This experiment presents a great deal of information on the low-temperature morphology and crystallography resulting from the martensitic transformation in sodium metal. The transformation is shown to produce a complex low-temperature structure with competition between several closely related phases. As sodium is warmed, following the transformation, it appears that it proceeds toward a hcp structure by adopting the long-period

"almost-hexagonal" approximates to this form. The appearance of these different phases is similar to the effects discussed by Bruinsma and Zangwill,[43,44] but does not appear to be driven by electron-density effects. Unfortunately, this experiment provides no additional evidence on transformation precursors or on candidates for its driving mechanism. For sodium metal, the mechanism of transformation remains an open question.

ACKNOWLEDGMENTS

Work at University of Missouri Research Reactor (MURR) was partially supported by the U.S. Department of Energy Grant No. DE-FG07-80ER10275. Additional support was provided by the Division of Materials Science, U.S. Department of Energy under Contract No. DE-AC05-840R21400 with Martin Marietta Energy systems, Inc. The work at John Carroll University was supported by NSF Grant No. DMR 88-19608. The authors acknowledge with pleasure the cooperation of the National Institute of Standards and Technology, which provided the spectrometer time for many of the neutron-diffraction measurements described here. These experiments produced a great deal of data that could not have been processed without the efforts of G. Moum, who designed and manages the MURR computer network. We also appreciate the assistance provided by T. Jokerst in the stacking-fault enumerations and L. Johnstone in the analysis of the diffraction data. The authors thank R. Ghosh of the Institut Laue-Langevin, who provided an extremely useful least-squares-fitting computer program, and W. B. Yelon and M. Seewoster for their comments on the manuscript.

[1]C. S. Barrett and O. R. Trautz, Trans. Am. Inst. Min. Metall. Pet. Eng. **175**, 579 (1948).
[2]C. S. Barrett, Acta Crystallogr. **9**, 671 (1956).
[3]Z. Nishiyama, *Martensitic Transformation* (Academic, New York, 1978).
[4]C. M. McCarthy, C. W. Thompson, and S. A. Werner, Phys. Rev. B **22**, 574 (1980).
[5]A. W. Overhauser, Phys. Rev. Lett. **53**, 64 (1984).
[6]R. Berliner and S. A. Werner, Phys. Rev. B **34**, 3586 (1986).
[7]G. Ernst, C. Artner, O. Blaschko, and G. Krexner, Phys. Rev. B **33**, 6485 (1986).
[8]H. G. Smith, Phys. Rev. Lett. **58**, 1228 (1987).
[9]R. Berliner, O. Fajen, H. G. Smith, and J. Jorgensen, Phys. Rev. B **40**, 12 086 (1989).
[10]R. Gooding and J. A. Krumhansl, Phys. Rev. B **38**, 1695 (1986).
[11]L. E. Tanner and M. Wuttig, Mater. Sci. Eng. A **127**, 137 (1990).
[12]L. E. Tanner, D. Schryvers, and S. M. Shapiro, Mater. Sci. Eng. A **127**, 205 (1990).
[13]E. C. Bain, Trans. Metall. Soc. AIME **70**, 25 (1924).
[14]O. Blaschko and G. Krexner, Phys. Rev. B **30**, 1667 (1984).
[15]G. Dolling, B. M. Powell, and P. Martel, Can. J. Phys. **46**, 1727 (1968).
[16]H. G. Smith, G. Dolling, R. M. Nicklow, P. R. Vijayaraghavan, and M. K. Wilkinson, *Inelastic Scattering of Neutrons in Solids and Liquids* (International Atomic Energy Agency, Vienna, 1963), Vol. 1, p. 149.
[17]H. G. Smith, R. Berliner, J. D. Jorgensen, M. Nielsen, and J. Trivisonno, Phys. Rev. B **41**, 1231 (1990).
[18]R. Stedman, J. Phys. F **6**, 2239 (1976).
[19]J. Trivisonno, A. R. Slotwinski, and M. P. Johnson, J. Phys. (Paris) Colloq. **42**, C5-983 (1981).
[20]J. Szente and J. Trivisonno, Phys. Rev. B **37**, 8447 (1988).
[21]W. B. Daniels, Phys. Rev. **119**, 1246 (1960).
[22]Mary E. Diederich and J. Trivisonno, J. Phys. Chem. Solids **27**, 637 (1966).
[23]The transverse width of the diffraction peak in reciprocal lattice units is given by $Q=2\pi h(\sqrt{2}/a)$ for the bcc (110) diffraction peaks, and $Q=4\pi h/(a\sqrt{3})$ for the 9*R* (001).
[24]M. L. Crow, G. Schupp, W. B. Yelon, J. G. Mullen, and A. Djedid, Phys. Rev. B **39**, 909 (1989).
[25]J. R. D. Copley and B. N. Brockhouse, Can. J. Phys. **51**, 657 (1973).
[26]The transformed fraction cannot be inferred from the bcc (110) intensity ratio decrease because of primary extinction effects in the untransformed crystal.
[27]A. H. Danne, R. E. Rundle, H. G. Smith, and F. H. Spedding, Acta. Crystallogr. **7**, 532 (1954).
[28]W. Schwartz, O. Blaschko, and I. Gorgas, Phys. Rev. B **44**, 6785 (1991).
[29]W. Schwartz and O. Blaschko, Phys. Rev. Lett. **65**, 3144 (1990).
[30]H. G. Smith (unpublished).
[31]H. G. Smith, R. Berliner, M. Nielsen, and J. Trivisonno (unpublished).
[32]The $N=6$ rhombohedral polytype is identical with the $N=3$ (fcc) stacking.
[33]A. R. Verma and P. Krishna, *Polymorphism and Polytypism in Crystals* (Wiley, New York, 1966).
[34]The subscript 3 in the Zhdanov symbol $(n_+,n_-)_3$ indicates that the stacking sequence is repeated three times to yield the complete rhombohedral unit cell.
[35]E. Michalski, Acta Crystallogr. A **44**, 640 (1988).
[36]E. Michalski, S. Kaczmarek, and M. Demianiuk, Acta Crystallogr. A **44**, 650 (1988).
[37]M. T. Sebastian and P. Krishna, Prog. Crys. Growth Charact. **14**, 103 (1987).
[38]M. T. Sebastian, Philos. Mag. B **57**, 93 (1988).
[39]A. D. Bruce and R. A. Cowley, *Structural Phase Transitions* (Taylor & Francis, London, 1981).
[40]R. Currat and R. Pynn, *A Treatise on Materials Science and Technology,* edited by G. Kostorz (Academic, New York, 1979).
[41]O. Blaschko, Mater. Sci. Eng. A **127**, 257 (1990).
[42]H. G. Smith, R. Berliner, J. D. Jorgenson, and J. Trivisonno, Phys. Rev. B **43**, 4524 (1991).
[43]R. Bruinsma and A. Zangwill, Phys. Rev. B **55**, 214 (1985).
[44]A. Zangwill, Comments Condens. Matter. Phys. **13**, 1 (1987).